the peak centered on SIR values usually represents only a small fraction of the total number of invariants (typically <10%), and they can be readily identified. We found that in these cases simply rejecting all estimates near the corresponding SIR invariants (within 5°) results in error distributions similar to those found in the general case. Thus it should still be possible to obtain unbiased protein phases from the remaining invariant estimates. It is useful to do this for all space groups even when the heavy-atom-invariant correction is included, except when the triplet consists of all centric reflections.

Summary

The procedure for estimating three-phase structure invariants from single isomorphous replacement data (Hauptman, 1982) as modified by Fortier, Moore & Fraser (1985) has been extensively tested on over 260 million invariants computed from 17 protein structures and 34 heavy-atom derivatives. It was found that the procedure can provide reasonably accurate values for any protein and derivative combination. Although the modification of Fortier greatly reduces systematic bias towards 'unresolved SIR values', a residual bias still remains. This residual bias can be further reduced, or eliminated, by one of several procedures described in this manuscript. If a correction term is added to account for the heavy-atom invariant, the accuracy is often improved as well. When applied to systems with heavy atoms in a centrosymmetric arrangement, the distribution of errors in the estimates is frequently bimodal, with the major peak centered on the true protein invariants and the minor peak on their SIR counterparts. The estimates near SIR values are readily identified and can be removed, leaving an acceptable distribution of errors in the remaining estimates. The new estimates, being unbiased with randomly distributed errors, should be better suited for use in phase-determining procedures.

Finally, it must be noted that although the procedures outlined can be used to reduce both the absolute errors and bias towards SIR inherent in the estimates, they do not resolve the twofold ambiguity in that there are still two equally probable estimates for each invariant. Work is under way in our laboratory and elsewhere (Hao Quan & Fan Hai-Fu, 1988; Klop, Krabbendam & Kroon, 1987; Langs, 1986; Fan Hai-Fu, Han Fu-son, Qian Jin-zi & Yao Jia-xing, 1984) to resolve this difficulty by various procedures.

The authors are grateful to Dr S. Fortier for helpful discussions. This work was supported by NIH grant GM32918-01A1.

References

BERNSTEIN, F. C., KOETZLE, T. F., WILLIAMS, G. J. B., MEYER, E. P. JR, BRICE, M. D., RODGERS, J. R., KENNARD, O., SHIMANOUCHI, T. & TASUMI, M. (1977). *J. Mol. Biol.* **112**, 535-542.

FAN HAI-FU, HAN FU-SON, QIAN JIN-ZI & YAO JIA-XING (1984). *Acta Cryst.* A**40**, 489-495.

FORTIER, S., MOORE, N. J. & FRASER, M. E. (1985). *Acta Cryst.* A**41**, 571-577.

FUREY, W. JR, WANG, B. C., YOO, C. S. & SAX, M. (1983). *J. Mol. Biol.* **167**, 661-692.

GIACOVAZZO, C., CASCARANO, G. & ZHENG, C. D. (1988). *Acta Cryst.* A**44**, 45-51.

HAN, F. & LANGS, D. A. (1988). *Acta Cryst.* A**44**, 563-566.

HAO QUAN & FAN HAI-FU (1988). *Acta Cryst.* A**44**, 379-382.

HAUPTMAN, H. (1982). *Acta Cryst.* A**38**, 289-294.

KARLE, J. (1983). *Acta Cryst.* A**39**, 800-805.

KLOP, E. A., KRABBENDAM, H. & KROON, J. (1987). *Acta Cryst.* A**43**, 810-820.

LANGS, D. A. (1986). *Acta Cryst.* A**42**, 362-368.

WANG, B. C., YOO, C. S. & SAX, M. (1979). *J. Mol. Biol.* **129**, 657-674.

XU, Z. B., YANG, D. S. C., FUREY, W. JR, SAX, M., ROSE, J. & WANG, B. C. (1984). Proc. Am. Crystallogr. Assoc. Meet., Lexington, Kentucky, 20-25 May 1984. Abstr. PC2, 50.

Acta Cryst. (1990). A**46**, 567-576

Phase Effects in Three-Beam Grazing-Incidence X-ray Diffraction

BY TZE-PING TSENG AND SHIH-LIN CHANG

Department of Physics, National Tsing Hua University, Hsinchu, Taiwan 30043

(*Received* 31 *October* 1989; *accepted* 28 *February* 1990)

Abstract

The effects of X-ray reflection phases on the surface-reflected intensity, the dispersion surface and the excitation of modes of wave propagation of three-beam grazing-incidence X-ray diffraction are investigated *via* numerical calculations, based on the dynamical theory. Possible ways of determining the triplet phases involved are demonstrated. The *Aufhellung* and *Umweganregung* interactions and the

0108-7673/90/070567-10$03.00

geometric effects due to crystal rotation are also discussed.

1. Introduction

The phase of an X-ray reflection is one of the main concerns in X-ray diffraction/scattering experiments. For single-crystal diffractions, it is well known that the phase can affect considerably the diffraction intensity of a multi-beam diffraction (*e.g.* Kambe & Miyake, 1954; Hart & Lang, 1961; Colella, 1974; Post, 1977; Chapman, Yoder & Colella, 1981; Høier & Aanestad, 1981; Chang, 1982; Juretschke, 1982; Hümmer & Billy, 1986; Shen & Colella, 1988; Mo, Haubach & Thorkildsen, 1988; Chang & Tang, 1988; Hümmer, Weckert & Bondza, 1989). In the case of grazing-incidence X-ray diffraction, abbreviated as GIXD (Marra, Eisenberger & Cho, 1979; Vineyard, 1982; Afanas'ev & Melkonyan, 1983; Cowan, 1985; Hoche, Brümmer & Nieber, 1986; Sakata & Hashizume, 1988; Fuoss, Liang & Eisenberger, 1989; Durbin & Gog, 1989; Hung & Chang, 1989), X-ray reflection phases should, in principle, also be involved in multi-beam diffraction processes. However, reports on this particular phase problem have not been found in the literature. It is therefore the aim of this paper to investigate theoretically the effects of phases on the dynamical scattering of three-beam GIXD. Numerical calculations, based on the dynamical theory of GIXD (Afanas'ev & Melkonyan, 1983), are carried out for the coordinates of the wavepoint on the dispersion surface, the excitation of the mode of wave propagation and the reflected intensities. They are all related to the triplet phases involved. From these calculations, a possible way of determining the phases is suggested. *Aufhellung* and *Umweganregung* effects (Renninger, 1937), which are usually encountered in three-beam diffractions from a crystal bulk, are also predicted for the specularly reflected intensities at the three-beam interaction positions.

2. Geometry of three-beam GIXD

Grazing-incidence X-ray diffraction takes place when an incident X-ray, with a glancing angle of incidence φ about several arc min, is diffracted by a Bragg plane, say H. Two surface-reflected beams as well as two Bragg diffracted beams are generated. For simplicity, if the reciprocal-lattice vector $\mathbf{h}$ of the H reflection lies in the plane of the crystal surface, the azimuthal rotation ψ around $\mathbf{h}$ will bring additional sets of planes, whose reciprocal-lattice vectors also lie in the crystal surface, to satisfy simultaneously Bragg's law. Thus, multi-beam GIXD occurs. Figs. 1(*a*) and (*b*) show schematically two possible three-beam GIXD situations. In Fig. 1(*a*), the three reciprocal-lattice points, O, H and G, lie in the plane of the crystal surface OHG. **OH** (=**h**) and **OG** (=**g**) are the reciprocal-lattice vectors of the H and G reflection involved. C is the centre of the triangle OHG. The point M is at the middle of OH. The half circle is the locus of the Laue point (entrance point) of the two-beam H reflection, rotating around **OH**. E is an entrance point on the semicircle such that $EO = EH = k = 1/\lambda$, λ being the X-ray wavelength. $\angle EOP$ and $\angle EMP$ are the incident angle φ and the azimuthal angle ψ, respectively.

The three-beam (O, H, G) GIXD takes place at E_3. $\mathbf{E_3O}$, $\mathbf{E_3H}$ and $\mathbf{E_3G}$ are the corresponding wavevectors $\mathbf{k}_0$, $\mathbf{k}_h$ and $\mathbf{k}_g$ outside the crystal. EP and E_3C are perpendicular to the crystal surface OHG. E_3' is the tie point, with respect to E_3, on the dispersion surface. The angles $\angle E_3OC$ and $\angle E_3MC$, denoted as φ_3 and ψ_3, are the incident angle and the azimuthal angle at the exact three-beam diffraction position, respectively. The corresponding reflection angle of the G reflection is φ_g. According to Hung & Chang (1989), if E_3 coincides with C, *i.e.* $\varphi_3 = 0$ and $\psi_3 = 0$, the intensity of the surface-reflected beam is null. Only those three-beam GIXD's with $\varphi_3 \neq 0$ and $\psi_3 \neq 0$, which have appreciable intensities, are physically meaningful. In the following discussion, we shall concentrate on this type of GIXD.

In Fig. 1(*a*), the centre C is inside the triangle OHG. If the ψ rotation is performed from E_1 to E_3, the three-beam GIXD at E_3 is in the 'OUT' situation because point G is moving away from E_3. In Fig. 1(*b*), point C is outside OHG. The three-beam case at E is in the 'IN' situation because point G is moving towards E_3 during the ψ rotation. It will become clear that the discrimination of the IN-OUT situation plays an important role in GIXD phase determination.

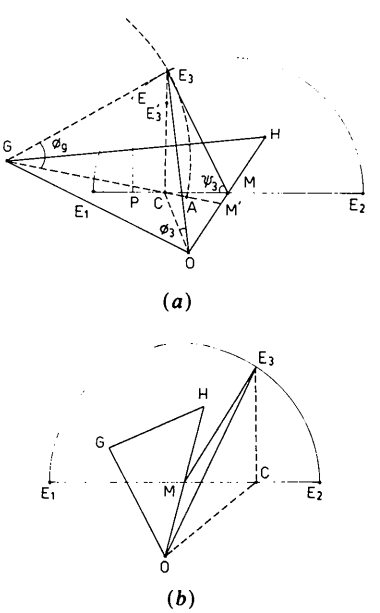

Fig. 1. Geometry of three-beam GIXD: (*a*) 'OUT' and (*b*) 'IN' situations.

As has been pointed out (Hung & Chang, 1989), the Bragg condition for a symmetric ($h = g = |\mathbf{g}-\mathbf{h}|$) three-beam GIXD can be written as

$$\lambda = 2d_h \sin\theta_h = 2d_h \sin(\pi/3)\cos\varphi_3 \qquad (1)$$

with

$$\cos\psi_3 = \tan\theta_h/\tan(\pi/3) \qquad (2)$$

where θ_h is the Bragg angle of the H reflection. d_h is the atomic spacing of the H reflection. For the angle of G reflection $\varphi_g = 0$, the corresponding incident angle $\varphi = \varphi_\Delta$ and the azimuth $\psi = \psi_\Delta$ are determined by (Hung & Chang, 1989)

$$\cos\psi_\Delta = 3\cos\psi_3 - 1/\cos\theta_h \qquad (3)$$

$$\sin\varphi_\Delta = \cos\theta_h \sin\psi_\Delta. \qquad (4)$$

For a general three-beam GIXD, the diffraction condition takes the following form:

$$\lambda = 2d_h \sin\angle OGH \cos\varphi_3 = 2d_h \sin\theta_h. \qquad (5)$$

The corresponding ψ_Δ for $\varphi_g = 0$ (*i.e.* where the wavefront of the G reflection cuts the crystal surface at point A) is the azimuthal angle at which EP is tangential to the sphere, centred at G, of radius k. Since ψ_3 is a small angle, ψ_Δ is defined approximately as

$$\cos\psi_\Delta \simeq [\cos\varphi_3 \cos\angle OGH - \sin^2\varphi_3/(2\cos\varphi_3 \cos t)]/\cos\theta_h \qquad (6)$$

where $t = \angle MCM'$ and ψ_3 is related to φ_3 as $\sin\varphi_3 = \cos\theta_h \sin\psi_3$. The wavelength λ used varies as the angle of incidence φ_3 changes. For a given λ, the incident angle φ varies during the ψ scan. The intensities of the surface-reflected beams, denoted as P_0^s, P_h^s and P_g^s, *versus* ψ are the diffraction profiles to be dealt with in this study.

3. Theoretical considerations

For a given three-beam (O, H, G) GIXD, the fundamental equation of wavefields for both σ and π polarizations can be expressed as

$$\begin{pmatrix} \chi_0-2\varepsilon_0 & 0 & p_\sigma\chi_{\bar h} & 0 & d_2\chi_{\bar g} & 0 \\ 0 & \chi_0-2\varepsilon_0 & 0 & p_\pi\chi_{\bar h} & d_1\chi_{\bar g} & d_3\chi_{\bar g} \\ p_\sigma\chi_h & 0 & \chi_0-2\varepsilon_h & 0 & d_2'\chi_{h-g} & 0 \\ 0 & p_\pi\chi_h & 0 & \chi_0-2\varepsilon_h & d_1\chi_{h-g} & d_3'\chi_{h-g} \\ d_2\chi_g & d_1\chi_{g-h} & d_2'\chi_{g-h} & d_1'\chi_{g-h} & \chi_0-2\varepsilon_g & 0 \\ 0 & d_3\chi_g & 0 & d_3'\chi_{g-h} & 0 & \chi_0-2\varepsilon_g \end{pmatrix} \begin{pmatrix} D_{\sigma 0} \\ D_{\pi 0} \\ D_{\sigma h} \\ D_{\pi h} \\ D_{\sigma g} \\ D_{\pi g} \end{pmatrix} = [0], \qquad (7)$$

where $\chi_g/4\pi$ is the electric susceptibility of the G reflection. $\chi_g = \Gamma F_g$, where $\Gamma = -r_e\lambda/\pi V$. F_g is the structure factor, r_e the classic radius of the electron and V the volume of the crystal unit cell. The quantity 2ε is defined as

$$2\varepsilon_L = (K_L^2 - k^2)/k^2 \qquad (8)$$

for $L = 0$, g and h. $\mathbf{K}_L$ is the wavevector of the L reflection inside the crystal. k is the magnitude of the wavevector in vacuum.

The D_σ's and D_π's are the σ- and π-polarized wavefields. The p's and d's are the polarization factors defined, according to Fig. 2, as

$$\begin{aligned} p_\sigma &= \hat{\boldsymbol{\sigma}}_0 \cdot \hat{\boldsymbol{\sigma}}_h & d_2 &= \hat{\boldsymbol{\sigma}}_0 \cdot \hat{\boldsymbol{\sigma}}_g & d_2' &= \hat{\boldsymbol{\sigma}}_g \cdot \hat{\boldsymbol{\sigma}}_h \\ p_\pi &= \hat{\boldsymbol{\pi}}_0 \cdot \hat{\boldsymbol{\pi}}_h & d_3 &= \hat{\boldsymbol{\pi}}_0 \cdot \hat{\boldsymbol{\pi}}_g & d_3' &= \hat{\boldsymbol{\pi}}_h \cdot \hat{\boldsymbol{\pi}}_g \\ & & d_1 &= \hat{\boldsymbol{\pi}}_0 \cdot \hat{\boldsymbol{\sigma}}_g & d_1' &= \hat{\boldsymbol{\pi}}_h \cdot \hat{\boldsymbol{\sigma}}_g \end{aligned} \qquad (9)$$

where all the $\boldsymbol{\sigma}$ unit vectors are chosen to be perpendicular to the crystal surface OGH. E_3' is the tie point on a branch of the dispersion surface. The difference E_3E_3' is the accommodation $k\delta$. $\mathbf{K}_0$ ($= \mathbf{E}_3'\mathbf{O}$), $\mathbf{K}_h$ ($= \mathbf{E}_3'\mathbf{H}$) and $\mathbf{K}_g$ ($= \mathbf{E}_3'\mathbf{G}$) are the wavevectors inside the crystal. The $\hat{\boldsymbol{\sigma}}$'s, $\hat{\boldsymbol{\pi}}$'s and $\mathbf{K}$'s satisfy the relation

$$\hat{\boldsymbol{\sigma}}_L = \hat{\mathbf{K}}_L \times \hat{\boldsymbol{\pi}}_L. \qquad (10)$$

Owing to grazing incidence, ψ_3 and φ_3 are very small so that the $\mathbf{k}$'s are almost parallel to the crystal surface. Thus the $\hat{\boldsymbol{\sigma}}$'s are approximately perpendicular to the surface. In these circumstances, the polarization factors become (see Fig. 2*b*)

$$\begin{aligned} &\hat{\boldsymbol{\sigma}}_i \cdot \hat{\boldsymbol{\pi}}_j = 0 && \hat{\boldsymbol{\sigma}}_i \cdot \hat{\boldsymbol{\sigma}}_j = 1 \\ &\hat{\boldsymbol{\pi}}_0 \cdot \hat{\boldsymbol{\pi}}_h \simeq \cos 2\theta_h && \hat{\boldsymbol{\pi}}_0 \cdot \hat{\boldsymbol{\pi}}_g \simeq \cos 2\theta_g \\ &\hat{\boldsymbol{\pi}}_g \cdot \hat{\boldsymbol{\pi}}_h \simeq \cos 2\theta_{g-h} \end{aligned} \qquad (11)$$

where θ_g, θ_h and θ_{g-h} are the Bragg angles of the G, H, and $G-H$ reflections, respectively. With this small-angle approximation, (7) can be decomposed

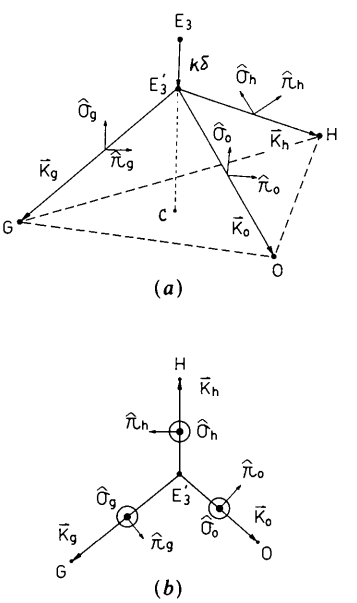

Fig. 2. Definition of the polarization unit vectors: (*a*) side view; (*b*) top view.

into two matrix equations of the form

$$\begin{pmatrix} \chi_0+\varphi^2-u^2 & p_h\chi_{\bar{h}} & p_g\chi_{\bar{g}} \\ p_h\chi_h & \chi_0+\varphi^2-u^2-\alpha_h & p_{g-h}\chi_{h-g} \\ p_g\chi_g & p_{g-h}\chi_{g-h} & \chi_0+\varphi^2-u^2-\alpha_g \end{pmatrix}\begin{pmatrix} D_0 \\ D_h \\ D_g \end{pmatrix}=(0), \tag{12}$$

where

$$p_{g-h}\simeq p_h=p_g=1$$

for σ polarization and

$$p_h=\cos 2\theta_h,\ p_g=\cos 2\theta_g,\ p_{g-h}=\cos 2\theta_{g-h}$$

for π polarization. The parameters φ, u, α_g and α_h are defined as

$$\begin{aligned} \varphi &= k_{0z}/k \qquad u = K_{0z}/k \\ \alpha_g &= [(\mathbf{k}_0+\mathbf{g})^2-k_0^2]/k^2 \\ \alpha_h &= [(\mathbf{k}_0+\mathbf{h})^2-k_0^2]/k^2 \end{aligned} \tag{13}$$

where K_{0z} is the vector component of $\mathbf{K}_0$ normal to the crystal surface.

Equation (12) can be solved as an eigenvalue problem. The determinant of the 3×3 matrix in (12) equal to zero is the dispersion equation, which is the necessary condition for (12) having non-trivial solutions. Since the H planes always satisfy the Bragg condition, $\alpha_h=0$. For simplicity, we only consider the σ-polarized wavefields in the following discussion. The dispersion equation can be expressed as

$$W^3-\alpha_g W^2+pW + (\alpha_g\chi_g\chi_{\bar{g}}+\chi_{\bar{h}}\chi_g\chi_{h-g}+\chi_h\chi_{\bar{g}}\chi_{g-h})=0, \tag{14}$$

where

$$W=\chi_0-u^2+\varphi^2 \tag{15}$$

$$p=-\chi_g\chi_{\bar{g}}-\chi_h\chi_{\bar{h}}-\chi_{g-h}\chi_{h-g}. \tag{16}$$

The real part of the eigenvalue gives the coordinates of the tie point on the dispersion surface, which defines the mode of propagation. The imaginary part determines the absorption. The eigenvectors provide the ratios among the amplitudes of the wavefields involved. The absolute wavefield amplitudes can be determined *via* the boundary conditions

$$E_0+E_0^s=\sum_{j=1}^{3}D_0(j) \tag{17a}$$

$$E_h^s=\sum_{j=1}^{3}D_h(j) \tag{17b}$$

$$E_g^s=\sum_{j=1}^{3}D_g(j) \tag{17c}$$

and

$$\varphi(E_0-E_0^s)=\sum_{j=1}^{3}u(j)D_0(j) \tag{18a}$$

$$-\varphi_h E_h^s=\sum_{j=1}^{3}u(j)D_h(j) \tag{18b}$$

$$-\varphi_g E_g^s=\sum_{j=1}^{3}u(j)D_g(j) \tag{18c}$$

for the continuities of the normal components of the electric displacements and the tangential components of the magnetic fields at the crystal boundary, respectively. E_0 is the incident wavefield amplitude. E_0^s, E_h^s and E_g^s are the amplitudes of the surface-reflected waves of the O, H and G reflections.

The corresponding intensities of the surface-reflected beams are then equal to

$$P_0^s=|E_0^s/E_0|^2 \tag{19a}$$

$$P_h^s=|E_h^s/E_0|^2(\varphi_h/\varphi) \tag{19b}$$

$$P_g^s=|E_g^s/E_0|^2(\varphi_g/\varphi). \tag{19c}$$

For a general three-beam GIXD, the eigenvalue equation (12) cannot be solved analytically. The eigenvalues, eigenvectors and the diffracted intensities can only be calculated numerically.

4. Phase effects on the dispersion relation

When the crystal is set at the exact three-beam GIXD diffraction position, $\varphi=\varphi_3$, $\psi=\psi_3$ and $\alpha_g=\alpha_h=0$. With the small-imaginary-part approximation (p and q are real), the dispersion equation (14) can be written as

$$W^3+pW+q=0 \tag{20}$$

where

$$W=\varphi_3^2+\chi_0-u^2 \tag{21}$$

$$p=-\chi_g\chi_{\bar{g}}-\chi_h\chi_{\bar{h}}-\chi_{g-h}\chi_{h-g} \tag{22}$$

$$q=\chi_h\chi_{\bar{g}}\chi_{g-h}+\chi_{\bar{h}}\chi_g\chi_{h-g}. \tag{23}$$

The roots W of (20) depend on the discriminant D_e defined as

$$D_e=-(4p^3+27q^2). \tag{24}$$

If $D_e<0$, there are one real and two complex conjugate roots. If $D_e=0$, there are two identical real roots. If $D_e>0$, there are three unequal real roots. For simplicity, if anomalous dispersion is not considered, then

$$\chi_{\bar{h}}=\chi_h^*,\quad \chi_{\bar{g}}=\chi_g^*,\quad \chi_{g-h}=\chi_{h-g}^*$$

where * denotes complex conjugate. p and q take the forms

$$p=-|\chi_g|^2-|\chi_h|^2-|\chi_{g-h}|^2 \tag{25}$$

$$q=-2|\chi_h\chi_{\bar{g}}\chi_{g-h}|\cos\delta_3 \tag{26}$$

where δ_3 is the phase of the structure-factor triplet $F_hF_{\bar{g}}F_{g-h}$. Since p and q are real, $D_e>0$. This means that W has three unequal real roots. Assume that these roots are α, β and γ.

(i) $\cos\delta_3>0$, $q<0$

$\alpha\beta\gamma>0$ because the sign of q determines the sign of $\alpha\beta\gamma$. Since the coefficient of W^2 is null, the sum of α, β and γ is always zero:

$$\alpha+\beta+\gamma=0. \tag{27}$$

Hence α, β and γ should have one positive and two negative in order to fulfil (27) and $\alpha\beta\gamma>0$.

(ii) $\cos\delta_3<0$, $q>0$

The conditions $\alpha+\beta+\gamma=0$ and $\alpha\beta\gamma<0$ hold. This implies that there are one negative and two positive real roots for W.

5. Calculations and results

Numerical calculations, following the theoretical consideration given in § 3, are carried out for (i) the strong three-beam (220)(202)/(02$\bar{2}$) diffraction of Ge at the 'OUT' position; (ii) the weak three-beam (222)(113)/(11$\bar{1}$) of Ge at the 'OUT' position; and (iii) the strong three-beam (220)(111)/(11$\bar{1}$) diffraction of Ge at the 'IN' position. The crystal surface planes are ($\bar{1}$11) for case (i) and ($\bar{1}$10) for (ii) and (iii). The atomic scattering factors, temperature factor and anomalous-scattering correction are taken from *International Tables for X-ray Crystallography* (1974). Table 1 lists the real part F' and the imaginary part F'' of the structure factors calculated for $\lambda=1{\cdot}60830$, 1·73224 and 1·88580 Å.

The purpose of choosing these cases for illustration is to reveal the effects of geometry and phases on the surface-diffracted intensity distributions, the dispersion surface and the excitation of the mode of wave propagation.

(i) Ge (000)(220)(202)/(02$\bar{2}$) OUT

This strong three-beam diffraction occurs at $\psi_3=22$ mrad ($\varphi_3=11$ mrad) for $\lambda=3{\cdot}464471$ Å. The ψ scan is around the reciprocal-lattice vector of the 220 reflection. For simplicity and for the purpose of illustration, we purposely choose the second harmonic, *i.e.* $\lambda=1{\cdot}732235$ Å, for calculation. The triplet phase $\delta_3=\delta_{220}+\delta_{\bar{2}0\bar{2}}+\delta_{0\bar{2}2}$ is 0°.

Figs. 3(*a*)-(*d*) show the surface-reflected intensities P^s_{000}, P^s_{220} and P^s_{202}, the dispersion surface (the real part of u, Re[u], *versus* ψ), the excitation Ex (i) of mode and the penetration depth t, respectively. The excitation, the penetration depth t_i and the average penetration depth $\bar{t}$ are defined as

$$\mathrm{Ex}\,(i)=\sum_{L=0,g,h} D^*_L(i)D_L(i)/|E_0|^2 \tag{28}$$

$$t_i=1/\{2\pi k\,\mathrm{Im}\,[u(i)]\} \tag{29a}$$

$$\bar{t}=\sum_{i=1}^{3} t_i\,\mathrm{Ex}\,(i), \tag{29b}$$

where Im stands for the imaginary part. As pointed out by Hung & Chang (1989), the secondary reflection

Table 1. *Calculated structure factors*

	1·60830 Å		1·73224 Å		1·88580 Å	
h k l	*F'*	*F''*	*F'*	*F''*	*F'*	*F''*
0 0 0	246·21	7·696	247·33	8·816	247·71	10·200
1 1 1	146·82	5·371	147·60	6·153	148·56	7·118
1 1 3	114·69	5·186	115·45	5·941	116·38	6·874
2 2 0	175·39	7·431	176·47	8·513	177·81	9·849
2 2 2	1·093	0·050	1·098	0·058	1·104	0·067

202 has a peak value in P^s_{202} at the ψ_Δ (=25·6 mrad) position (Fig. 3*a*). P^s_{000} and P^s_{220} have their usual characteristics as in the two-beam GIXD, except for a small modulation near ψ_3.

Fig. 3(*b*) is the intersection of the dispersion surface with the plane perpendicular to and bisecting the reciprocal-lattice vector of the 220 reflection. The dispersion curve of mode 1 follows the wavefront of the 202 reflected wave for $\psi<\psi_3$. At $\psi=\psi_3$, mode 1 intercepts with the dispersion curves of the two-beam 220 reflection. Modification of the dispersion

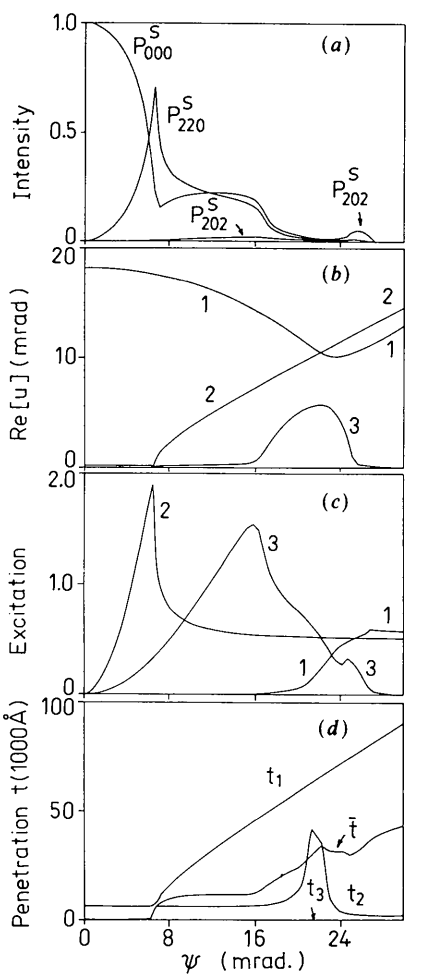

Fig. 3. Three-beam Ge (000, 220, 202) 'OUT' GIXD for $\lambda=1{\cdot}732235$ Å, $\delta_3=0°$ and $\psi_3=22$ mrad: calculated (*a*) intensities; (*b*) dispersion surface (the abscissa represents the crystal surface); (*c*) mode excitations; (*d*) penetration depths.

curves at ψ_3 takes place according to the phase effect mentioned in (20). Since $\chi_{220}=\chi_{202}=-\chi_{02\bar{2}}$, the dispersion equation (14) becomes

$$(W+\chi_{220})(W+\chi_{220})(W-2\chi_{220})=0 \qquad (30)$$

where

$$u^2=\varphi_3^2+\psi_0-W. \qquad (31)$$

Thus $u(1)=u(2)=(\varphi_3^2+\chi_0+\chi_{220})^{1/2}$, $u(3)=(\varphi_3^2+\chi_0-2\chi_{220})^{1/2}$ and $u(1)>u(3)$. Mode 1 and mode 2 are therefore degenerate at ψ_3. The dispersion curve of mode 3 is lower than those of modes 1 and 2. This is the characteristic of the dispersion curves for $\delta_3=0°$ ($\cos\delta_3>0$).

The excitations, Ex (2) and Ex (3), of modes 2 and 3 resemble those for two-beam (220) GIXD (*e.g.* Hung & Chang, 1989) for $\psi<\psi_3$. The excitation of mode 1 is almost zero for $\psi<\psi_3$. Near ψ_3, Ex (1) gradually increases, and reaches the two-beam value of Ex (3) for $\psi\gg\psi_3$. For $\psi\sim\psi_3$, Ex (3) decreases and a kink occurs near ψ_Δ. Ex (3) reaches zero for $\psi\gg\psi_3$. The excitation of mode 2 remains unaffected for all ψ. This means that mode 2 maintains its two-beam characteristics.

The penetration depths t of modes 1, 2 and 3 are shown in Fig. 3(*d*). t_1 is actually the penetration depth of the 220 reflected beam. Since Ex (1) has appreciable values only for $\psi\geq\psi_3$, t_1 contributes very little to the resultant penetration depth $\bar{t}$ for $\psi<\psi_\Delta$. t_2 has zero value for $\psi<\theta_1$ (=7·4 mrad, the critical angle of mode 2) because mode 2 is not excited in this angular range. Maximal penetration depth for mode 2 takes place near ψ_3 owing to the three-beam interaction. Mode 3 has very small penetration depth (<500 Å). The maximum for t_3 also occurs near ψ_3. The resultant penetration depth $\bar{t}$, according to (29*b*), has zero value for $\psi<\theta_1$ and increases gradually as ψ increases. A kink (~34 000 Å) in $\bar{t}$ is seen at ψ_3.

If a smaller ψ_3 (*i.e.* a longer wavelength) is chosen, P^s_{202} has less appreciable intensity at ψ_3. Similarly, the intersection of the dispersion surface due to the three-beam interaction occurs at ψ_3. The general behaviour of P^s_{000}, P^s_{220}, P^s_{202}, the dispersion surface, the excitation and the penetration depth, have been reported previously (Hung & Chang, 1989).

To reveal the phase effects on the calculation, the sign of the structure factor F_{202} is altered so that $\delta_3=180°$. Figs. 4(*a*)-(*c*) are the calculated results for the three-beam (OUT) case with $\psi_3=2$ mrad and $\delta_3=180°$. The surface-reflected intensities P^s_{000}, P^s_{220} and P^s_{202} resemble those for $\delta_3=0°$, except that P^s_{202} has a small kink near θ_1 (=7·4 mrad) for this case while the kink appeared near θ_2 (=16 mrad, the critical angle of mode 3) for $\delta_3=0°$. In addition, if we blow up P^s_{000} and P^s_{220} near ψ_Δ (=25·6 mrad), striking differences in the intensities appear between $\delta_3=0$ and $\delta_3=180°$ (Fig. 5). For $\delta_3=0°$, P^s_{000} and P^s_{220} seem to appear 'in phase', while they are 'out of phase' for $\delta_3=180°$.

The dispersion surface for $\delta_3=180°$ is shown in Fig. 4(*b*). According to (14), the dispersion relation can be written as

$$(W-\chi_{220})^2(W+2\chi_{220})=0. \qquad (32)$$

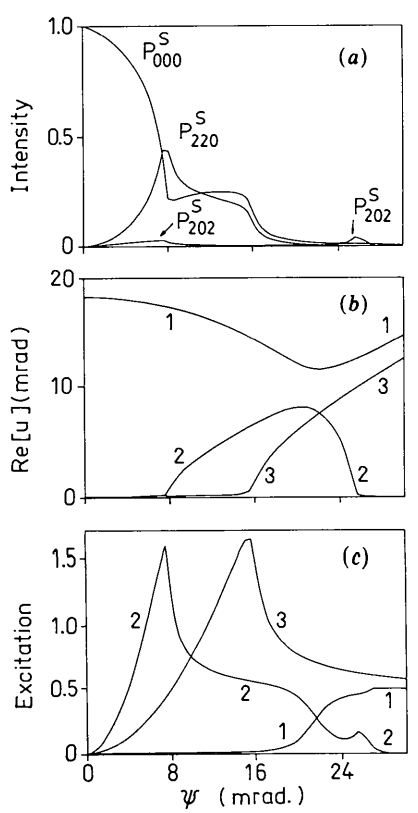

Fig. 4. Three-beam Ge (000, 220, 202) 'OUT' GIXD for λ = 1·732235 Å, $\delta_3=180°$ and $\psi_3=22$ mrad: calculated (*a*) intensities; (*b*) dispersion surface; and (*c*) mode excitations.

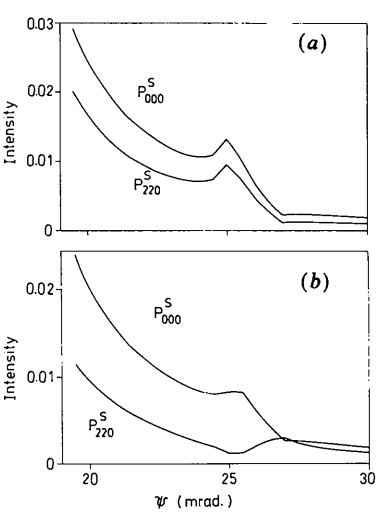

Fig. 5. Detailed intensity distributions of Figs. 3(*a*) and 4(*a*) near the intensity tails for (*a*) $\delta_3=0°$ and (*b*) $\delta_3=180°$, respectively.

Since $u^2=\varphi_3^2+\chi_0-W$, $u(1)=(\varphi_3^2+\chi_0+2\chi_{220})^{1/2}$, $u(2)=u(3)=(\varphi_3^2+\chi_0-\chi_{220})^{1/2}$ and $u(1)>u(2)$ at $\psi=\psi_3$ and $\varphi=\varphi_3$. Now the degeneracy takes place for mode 2 and mode 3. The relative position of the dispersion curve of mode 2 is different from that shown in Fig. 3(*b*) for $\delta_3=0°$. Mode 2 is located closer to mode 3 for $\delta_3=180°$ while mode 2 is closer to mode 1 for $\delta_3=0°$. Naturally, this difference causes differences in excitation. At ψ_3, the excitations are Ex (3) > Ex (2) > Ex (1) for $\delta_3=180°$. For $\delta_3=0°$, Ex (2) > Ex (3) > Ex (1). In the present case, mode 2 maintains its two-beam value, 50%, near ψ_3 and has a kink at ψ_Δ. Ex (1) is similar to the excitation of mode 1 shown in Fig. 3(*c*). Since the penetration depths resemble those for $\delta_3=0°$, they are not shown here.

(ii) Ge (000)(222)(113)/(11$\bar{1}$) OUT

This case involves a very weak symmetric 222 reflection. The triplet phase is $\delta_3=180°$. Figs. 6 and 7 are the calculations for $\psi_3=57{\cdot}4$ mrad ($\lambda=1{\cdot}608249$ Å) and $\psi_3=32$ mrad ($\lambda=1{\cdot}608305$ Å), respectively.

In Fig. 6(*a*), P^s_{222} has two peaks: one at the critical angle of mode 2, θ_1(=32 mrad), and the other at ψ_Δ (≃64 mrad). The peak intensities are as low as 0·004 owing to the weak 222 reflection. P^s_{113} has a kink near θ_1 and has appreciable intensity at ψ_Δ. It should be noted that the peak intensity of P^s_{113} near θ_1 is slightly higher than P^s_{222} near ψ_Δ. The sharp edge for P^s_{113} is due to the cut off of the 113 reflected beam at ψ_Δ. The P^s_{000} intensity (which is over the scale) is too high to be shown here. P^s_{000} has the same behaviour as in Figs. 3 and 4.

The phase effect on the dispersion surface is difficult to see in Fig. 6(*b*) at $\psi_3=0{\cdot}057$ mrad because of the weak three-beam interaction ($F_{222}\simeq 0$). There is no degeneracy in this case, *i.e.* no intersection among the dispersion curves at ψ_3, since the reciprocal-lattice vectors involved do not form a right triangle. The spacing between the dispersion curves of modes 2 and 3 is very small at ψ_3. This is mainly due to the smallness in the structure factor F_{222}.

The excitations of modes, shown in Fig. 6(*c*), resemble those shown in Fig. 4(*c*). The penetration depths t_2 and $\bar{t}$ have maximal values, about 1800 and 5500 Å, respectively at ψ_3 (Fig. 6*d*). This is due mainly

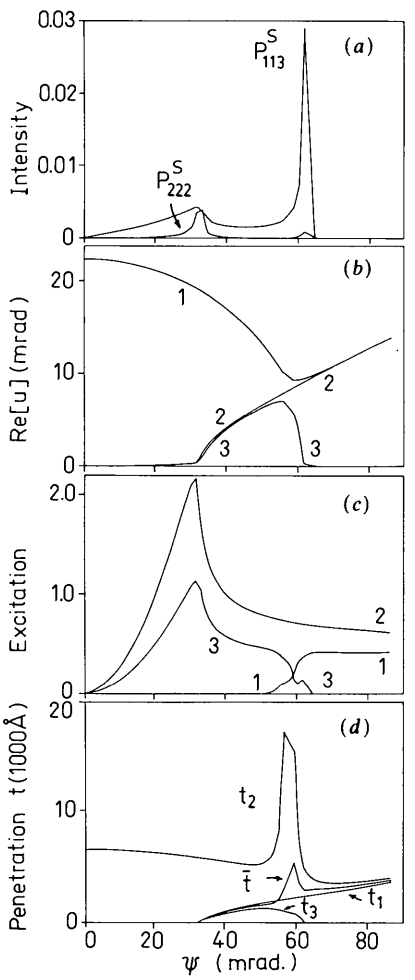

Fig. 6. Three-beam Ge (000, 222, 113) 'OUT' GIXD for $\lambda=1{\cdot}608305$ Å, $\delta_3=180°$ and $\psi_3=57{\cdot}4$ mrad: calculated (*a*) intensities; (*b*) dispersion surface; (*c*) mode excitations; and (*d*) penetration depths.

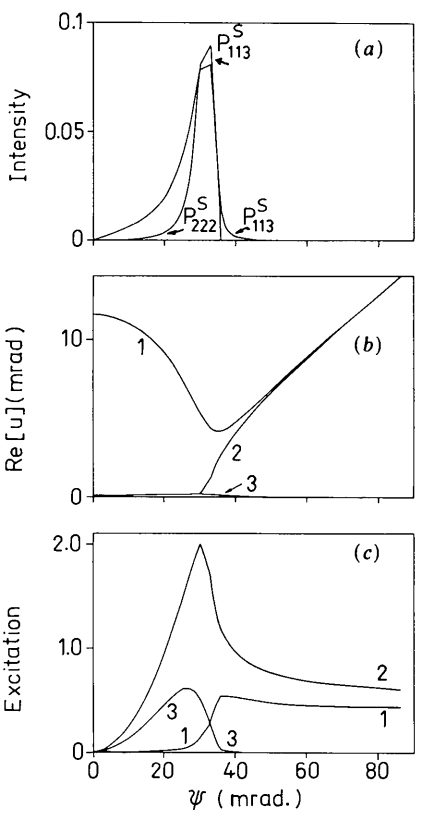

Fig. 7. Three-beam Ge (000, 222, 113) 'OUT' GIXD for $\lambda=1{\cdot}608290$ Å, $\delta_3=180°$ and $\psi_3=32$ mrad: calculated (*a*) intensities; (*b*) dispersion surface; (*c*) mode excitations.

to the weak 222 reflection, because the smaller the structure factor, the shorter the penetration for surface diffraction.

If we choose ψ_3 equal to 32 mrad ($\lambda = 1{\cdot}608290$ Å), the surface-reflected intensities P^s_{222} and P^s_{113} (see Fig. 7*a*) increase one order of magnitude higher than those shown in Fig. 6. The intensity P^s_{113} is still greater than P^s_{222} at ψ_3.

The dip of the dispersion curve of mode 1 is located at ψ_3, while the dispersion curve of mode 3 is almost invisible in Fig. 7(*b*).

The excitation Ex (2) of mode 2 has a two-beam character as ψ varies, while Ex (3) and Ex (1) behave like those for the case with $\psi_3 = 57$ mrad (Fig. 7*c*). The penetration depths of this case, resembling those shown in Fig. 6(*d*), are not shown in Fig. 7.

When the sign of F_{222} is changed from positive to negative, the corresponding δ_3 becomes 0°. Fig. 8 shows the calculated results for this artificial three-beam GIXD, with $\psi_3 = 57{\cdot}4$ mrad. The dispersion surface, shown in Fig. 8(*b*), and the excitation of modes, shown in Fig. 8(*c*), are the same as those shown in Fig. 6 for $\delta_3 = 180°$, because the weak three-beam interaction is not able to bring out the slight modification due to the phase on the dispersion surface. It is therefore not surprising to have the same dispersion and excitation for both $\delta_3 = 0$ and $\delta_3 = 180°$. However, as the phase angle changes from 180 to 0°, the intensities, which are also closely related to absorption, do exhibit different features. For example, in Fig. 8(*a*), the peak intensity of P^s_{222} is higher than that of P^s_{113} at θ_1 (=32 mrad). This is opposite to that shown in Fig. 6(*a*) for P^s_{222} and P^s_{113} near the same angular position. Similarly, if ψ_3 is set at 32 mrad ($\lambda = 1{\cdot}608305$ Å), the fact that $P^s_{222} > P^s_{113}$ at ψ_3 is also seen in Fig. 9(*a*). The dispersion surface and excitation of modes (Figs. 9*b* and *c*) are the same as those shown in Figs. 7(*b*) and (*c*).

(iii) Ge (000)(220)(111)/(11$\bar{1}$) IN

The three-beam case is an 'IN' GIXD, with the ψ rotation around the reciprocal-lattice vector of the 220 reflection. This 'IN' means that the reciprocal-lattice point of the 111 reflection is initially outside the Ewald sphere and is now brought onto the surface of the Ewald sphere *via* the ψ scan (See Fig. 1*b*).

The surface-reflected intensities P^s_{000}, P^s_{220} and P^s_{111} for $\delta_3 = 0°$ and $\psi_3 = 36$ mrad ($\lambda = 1{\cdot}885798$ Å) are

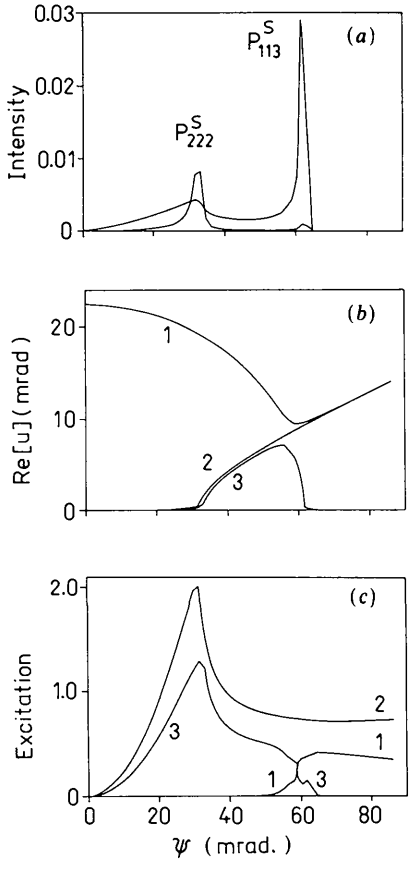

Fig. 8. Three-beam Ge (000, 222, 113) 'OUT' GIXD for $\lambda = 1{\cdot}608305$ Å, $\delta_3 = 0°$ and $\psi_3 = 57{\cdot}4$ mrad: calculated (*a*) intensities; (*b*) dispersion surface; (*c*) mode excitations.

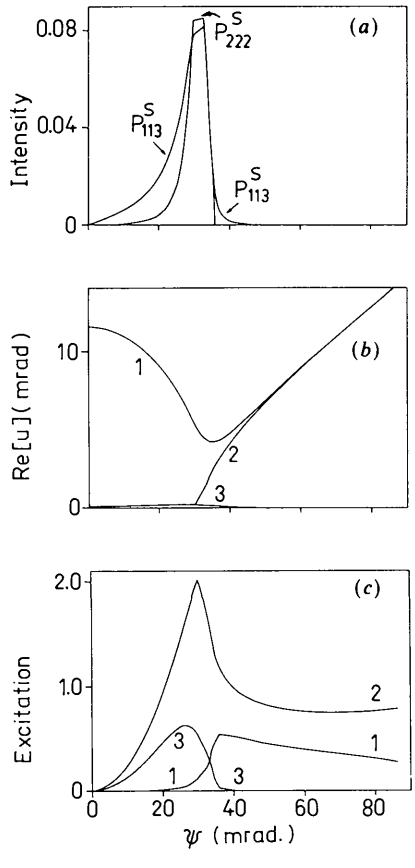

Fig. 9. Three-beam Ge (000, 222, 113) 'OUT' GIXD for $\lambda = 1{\cdot}608290$ Å, $\delta_3 = 0°$ and $\psi_3 = 32$ mrad: calculated (*a*) intensities; (*b*) dispersion surface; (*c*) mode excitations.

shown in Fig. 10(*a*). For $\psi < \psi_3$, P^s_{000} and P^s_{220} have similar behaviour as in two-beam GIXD. Near ψ_3 (almost at the critical angle of mode 3, $\theta_2 \sim 32$ mrad), the P^s_{111} has a kink. The sense of asymmetry of this intensity profile near ψ_3 is somewhat opposite to that shown in Fig. 3(*a*) for the three-beam (000)(220)(202)/(02$\bar{2}$) IN with $\delta_3 = 0°$. It is also true for the profiles of P^s_{000} and P^s_{220} near ψ_3. Figs. 11(*a*) and (*b*) are the detailed intensity distributions of P^s_{000} and P^s_{220} near ψ_3 for $\delta_3 = 0$ and 180°, respectively. The asymmetry of the intensity profiles is reversed as δ_3 varies from 0 to 180° (see also Fig. 5 for comparison).

Fig. 10(*b*) is the dispersion surface for the aforementioned IN three-beam case. The dispersion curves of modes 1 and 3 which have their two-beam characteristics are modified by the presence of the curve of mode 2, which is attributed to the 111 reflection. The phase effect on the relative location of the dispersion curves at ψ_3 is also seen as predicted by (14). The excitation of mode 1, Ex (1), exhibits its two-beam excitation for $\psi < \psi_3$. Near ψ_3, Ex (1) has a kink at θ_2 and then approaches 50% for $\psi \gg \psi_3$. Ex (3) also shows its two-beam excitation for $\psi < \psi_3$ and decreases as ψ increases. Ex (2) is almost zero for $\psi < \psi_3$ and approaches 50% for $\psi > \psi_3$.

The penetration depths, shown in Fig. 10(*d*), are very similar to those in Fig. 3(*d*), except that t_2 shows a broad peak feature on the higher-angle side. This results from the distortion of the dispersion towards the high angles in ψ.

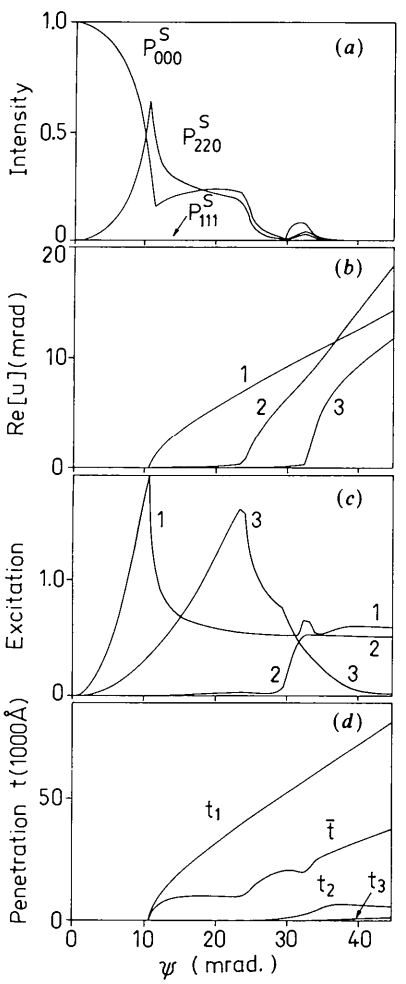

Fig. 10. Three-beam Ge (000, 220, 11) 'IN' GIXD for $\lambda =$ 1·885798 Å, $\delta_3 = 0°$ and $\psi_3 = 36$ mrad: calculated (*a*) intensities; (*b*) dispersion surface; (*c*) mode excitations; (*d*) penetration depths.

6. Discussion and concluding remarks

The three-beam GIXD's discussed above are of the Laue type, because the diffracting planes involved are perpendicular to the crystal surface. For strong three-beam interaction, in which strong reflections are involved, it is anticipated that the relative positions of the dispersion curves will be affected by the triplet phase, as has been reported for three-beam Borrmann diffractions (Post, 1977). For a weak three-beam interaction, such an arrangement of dispersion curves is less affected by the phase because the very weak reflection is chosen for the ψ rotation. In both strong and weak three-beam GIXD's, the surface-reflected intensities, as demonstrated in Figs. 5 and 11, indeed convey the phase information: For strong interactions, the synchronization of P^s_0 and P^s_h, *i.e.* 'in phase', near ψ_3 indicates that δ_3 is 0°; while for $\delta_3 = 180°$, P^s_0 and P^s_h are 'out of phase'. For weak interactions, these kinds of in phase and out of phase of P^s_0 and P^s_h are too weak to be detected. The phase information is, however, inherent in the relative intensity of P^s_h with respect to P^s_g. That is, for $\delta_3 = 0°$, $P^s_h > P^s_g$ at the critical angle θ_1, while $P^s_h < P^s_g$ for $\delta_3 = 180°$ at the same position.

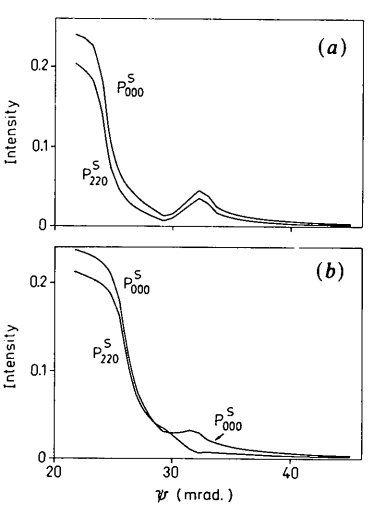

Fig. 11. Detailed intensity distributions of Fig. 10(*a*) near $\psi_3 =$ 36 mrad for (*a*) $\delta_3 = 0°$ and (*b*) $\delta_3 = 180°$.

The geometry related to the IN and OUT situations for multiple GIXD is also important to understand the phase effect on the surface-reflected intensities. As shown in Figs. 5 and 11, the sense of asymmetry of P_0^s and P_h^s for the IN situation is the reverse of that for the OUT situation. This is similar to the geometric effect on the intensity of a three-beam diffraction from a crystal bulk (Chang, 1982).

It is also worth noting that for the strong primary reflection like the 220 in the case $(000)(220)(202)/(02\bar{2})$, the P_{220}^s near ψ_3 is much weaker than the P_{220}^s for $\psi < \psi_3$, while for the weak primary reflection 222, the P_{222}^s at ψ_3 and especially at θ_1 has much higher intensity than the usual two-beam (222) GIXD intensity. As ψ_3 is closer to θ_1, the peak intensity P_{222}^s increases in order of magnitude. These two situations resemble the *Aufhellung* and *Umweganregung*, respectively, in ordinary multiple diffractions from bulk crystals (Renninger, 1937).

As has been demonstrated, both surface *Aufhellung* and *Umweganregung* seem to be useful in centric phase determination from the detection of the surface-reflected intensity variation.

The authors are indebted to the National Science Council for financial support under grant NSC 79-0204-M007-05. One of us, TPT, thanks the same organization for providing a graduate fellowship during the course of this study and H. H. Hung for useful discussions.

References

AFANAS'EV, A. M. & MELKONYAN, M. K. (1983). *Acta Cryst.* A**39**, 207-210.
CHANG, S. L. (1982). *Phys. Rev. Lett.* **48**, 163-166.
CHANG, S. L. & TANG, M. T. (1988). *Acta Cryst.* A**44**, 1065-1072.
CHAPMAN, L. D., YODER, D. R. & COLELLA, R. (1981). *Phys. Rev. Lett.* **46**, 1578-1581.
COLELLA, R. (1974). *Acta Cryst.* A**30**, 413-423.
COWAN, P. L. (1985). *Phys. Rev. B*, **32**, 5437-5439.
DURBIN, S. M. & GOG, T. (1989). *Acta Cryst.* A**45**, 132-141.
FUOSS, P. H., LIANG, K. S. & EISENBERGER, P. (1989). *Synchrotron Radiation Research: Advances in Surface Science*, edited by R. Z. BACHRACH. New York: Plenum.
HART, M. & LANG, A. R. (1961). *Phys. Rev. Lett.* **7**, 120-121.
HOCHE, H. R., BRÜMMER, O. & NIEBER, J. (1986). *Acta Cryst.* A**42**, 585-587.
HØIER, R. & AANESTAD, A. (1981). *Acta Cryst.* A**37**, 787-794.
HÜMMER, K. & BILLY, H. W. (1986). *Acta Cryst.* A**42**, 127-133.
HÜMMER, K., WECKERT, E. & BONDZA, H. (1989). *Acta Cryst.* A**45**, 182-187.
HUNG, H. H. & CHANG, S. L. (1989). *Acta Cryst.* A**45**, 823-833.
International Tables for X-ray Crystallography (1974). Vol. IV. Birmingham: Kynoch Press. (Present distributor Kluwer Academic Publishers, Dordrecht.)
JURETSCHKE, H. J. (1982). *Phys. Rev. Lett.* **48**, 1487-1489.
KAMBE, K. & MIYAKE, S. (1954). *Acta Cryst.* 7, 218-219.
MARRA, W. C., EISENBERGER, P. & CHO, A. Y. (1979). *J. Appl. Phys.* **50**, 6927-6933.
MO, F., HAUBACH, B. C. & THORKILDSEN, G. (1988). *Acta Chem. Scand. Ser. A*, **42**, 130-138.
POST, B. (1977). *Phys. Rev. Lett.* **39**, 760-763.
RENNINGER, M. (1937). *Z. Phys.* **106**, 141-176.
SAKATA, O. & HASHIZUME, H. (1988). *Jpn. J. Appl. Phys.* **27**, L1976-L1979.
SHEN, Q. & COLELLA, R. (1988). *Acta Cryst.* A**44**, 17-21.
VINEYARD, G. H. (1982). *Phys. Rev. B*, **26**, 4146-4159.

Acta Cryst. (1990). A**46**, 576-584

The Intensity Distribution Observed with a Multi-Crystal X-ray Diffractometer

BY E. L. GARTSTEIN

Department of Physics, University of Edinburgh, Mayfield Road, Edinburgh EH9 3JZ, Scotland, and Neeve Shaanan, Str. Berl Katzenelson 56/4, Haifa, Israel

AND R. A. COWLEY

Department of Physics, University of Edinburgh, Mayfield Road, Edinburgh EH9 3JZ, Scotland, and Clarendon Laboratory, University of Oxford, Parks Road, Oxford, England

(*Received* 17 *October* 1989; *accepted* 17 *March* 1990)

Abstract

Expressions are obtained for the intensity distributions which are observed when Bragg reflections are studied using an X-ray multi-crystal diffractometer. The expressions are obtained for both Bragg and Laue geometry at the sample, and assuming that the monochromator, sample and analyser elements are all perfect crystals. Detailed calculations are made of several configurations with both laboratory-based and synchrotron sources, and the results are compared with experimental measurements. The comparison shows that the theory gives reliable results not only for the half-widths of the distributions, but also for the tails of the distributions resulting from the dynamical effects in one or more of the crystals.

0108-7673/90/070576-09$03.00